Separation Science and Technology
Publication details, including instructions for authors and subscription information:
http://www.informaworld.com/smpp/title~content=t713708471

Line Shapes in Gas Chromatography. II. Nonlinear Isotherms and Mass Transfer Kinetics in Preparative Columns

David J. Wilson[a]
[a] Department of Chemistry, Vanderbilt University, Nashville, Tennessee

To cite this Article Wilson, David J.(1986) 'Line Shapes in Gas Chromatography. II. Nonlinear Isotherms and Mass Transfer Kinetics in Preparative Columns', Separation Science and Technology, 21: 9, 887 — 903
To link to this Article: DOI: 10.1080/01496398608058385
URL: http://dx.doi.org/10.1080/01496398608058385

SEPARATION SCIENCE AND TECHNOLOGY, **21**(9), pp. 887-903, 1986

Line Shapes in Gas Chromatography. II. Nonlinear Isotherms and Mass Transfer Kinetics in Preparative Columns

DAVID J. WILSON

DEPARTMENT OF CHEMISTRY
VANDERBILT UNIVERSITY
NASHVILLE, TENNESSEE 37235

Abstract

The effects of nonlinear isotherms and mass transfer kinetics on the shapes of bands in preparative gas chromatography are modeled by numerical integration of the differential equations describing solute movement. Numerical dispersion, intrinsic to the theoretical plate method, is greatly reduced by the use of asymmetrical upwind algorithms for advection. Mass transfer rate effects are taken into account by a time constant approach. The technique is readily used on microcomputers.

INTRODUCTION

The calculation of line shapes in gas chromatography has been of interest for many years, and is of particular interest in preparative columns where heavy liquid loadings on the column packing and large sample sizes make nonideal behavior a very common phenomenon. Since the pertinent literature was reviewed in an earlier paper (*1*), we here mention only those articles most directly relevant to our work.

Vink (*2, 3*) has used a mesh technique for solving the partial differential equation governing line shapes; our approach here is similar. Houghton took the effects of diffusion and nonequilibrium mass transport into account by means of a perturbation method (*4*). Giddings has developed a general method for line-shape calculations by means of a stochastic approach (*5*). We examined the effect of the finite rate of

 0149-6395/86/2109-0887$3.50/0

mass transport between the moving and stationary phases by means of a time-constant approach (*6*). Another paper of ours considered the effects of velocity and diffusion constant variation along the column length, the finite rate of mass transport, departures of the solute from Henry's law behavior, and finite sample injection time (*7*).

Of particular interest is the elegant paper on line shapes by Guiochon and his coworkers (*8*). Their model, based on the solution of the appropriate differential equation, permits them to account for both the influence of the isotherm curvature at zero concentration and the perturbation of the flow rate due to solute exchange between the mobile and stationary phases. The model requires peak area, axial dispersion coefficient, limit retentional time, and leaning coefficient. The last two parameters are directly related to the slope and curvature of the isotherm at the zero pressure limit. The method is good for low to moderate column overloading. It takes kinetic effects into account by a global dispersion factor, and neglects the kinetics of the adsorption-desorption process.

In the model to be examined here, we deal with conditions of large overload with nonlinear adsorption isotherms, and include the effect of the finite rate of mass transfer in the adsorption-desorption process. The nonlinearity of the equations dictates the numerical integration of the partial differential equation describing the system. This is made difficult by two factors. First, if the column is to be realistically efficient, a very large number of theoretical transfer units will be required. This means that one must numerically integrate a very large number of ordinary differential equations forward in time. Since the stability of this integration is determined by the requirement that $v\Delta t/\Delta x$ be <1, where v = flow velocity and Δx = theoretical plate height, the allowed values of Δt are also very small. This makes numerical integration a slow and costly business.

Actually, the situation is even worse than indicated above. The second factor adding to the difficulty of numerical integration methods comes into play if one wishes to include the effects of the finite rate of solute transport between phases and eliminate the assumption of local equilibrium. The time constant τ for this mass transport is quite short, and, if one is to solve the coupled partial differential equations describing the vapor and liquid phase concentrations of the solute, one must select values of Δt which are small compared to this small time constant. At this point one concludes that the outlook for numerical integration methods is not bright. It is these difficulties we wish to address.

The large number of theoretical plates required to represent a reasonably efficient column is closely related to the problem of numer-

ical dispersion in the simple mesh approximation to the advection term,

$$T_{\text{adv}} = -\frac{\partial}{\partial x}(vc_g) \tag{1}$$

where v = volumetric flow rate of gas at x
$c_g(x,t)$ = solute concentration in the vapor phase

Leonard (*9, 10*) has analyzed in some detail the advantages of using so-called asymmetrical upwind algorithms for modeling advection terms with very markedly reduced numerical dispersion, and we have exploited his suggestion in a number of applications (*1, 11–13*). The formulas used to approximate the advection term in our differential equation,

$$\frac{\partial m}{\partial t}(x,t) = A\frac{\partial}{\partial x}\left(D\frac{\partial c_g}{\partial x}\right) - \frac{\partial}{\partial x}(vc_g) \tag{2}$$

are

$$T_{\text{adv}} = (\mathrm{v}/\Delta x)(c_{g,i-1} - c_{g,i}) \tag{3}$$

$$= (\mathrm{v}/\Delta x)(-\tfrac{1}{2}c_{g,i-2} + 2c_{g,i-1} - \tfrac{3}{2}c_{g,i}) \tag{4}$$

$$= (\mathrm{v}/\Delta x)(-\tfrac{1}{8}c_{g,i-2} + \tfrac{7}{8}c_{g,i-1} - \tfrac{3}{8}c_{g,i} - \tfrac{3}{8}c_{g,i+1}) \tag{5}$$

$$= (\mathrm{v}/\Delta x)(-\tfrac{1}{6}c_{g,i-2} + c_{g,i-1} - \tfrac{1}{2}c_{g,i} - \tfrac{1}{3}c_{g,i+1}) \tag{6}$$

where $m(x,t)$ = moles of solute per unit length of column
v = linear velocity of vapor phase
A = cross-sectional area of column
D = axial dispersion constant
Δx = length of the compartments into which the column is partitioned

Representing the advective term in Eq. (2) by Eqs. (4), (5), or (6) eliminates the interpretation of each compartment representing the column as a theoretical plate, and results in drastically reduced numerical dispersion, as shown earlier (*1*). This, in turn, permits a much smaller number of compartments to be used in representing the column than would be required by the theoretical plate model.

Numerical integration would still be of dubious feasibility, however, if one were forced to use values of Δt dictated by the small size of the time

constant in the mass transfer of solute between the vapor and liquid phases. To deal with this we employ a modification of a method we used earlier to get fast-computing models for activated carbon columns (*14*) and continuous-flow solvent sublation columns (*15*). In any one compartment, one assumes an exponential decay of the liquid and vapor concentrations toward their local equilibrium values during the time increment Δt. The time constant for this decay can then be assigned on the basis of the solute diffusion constant in the liquid phase and the thickness of the liquid phase. If one numerically integrates the differential equations for c_g and c_l, the solute concentration in the liquid phase, directly, one is in essence assuming a linear change of the liquid and vapor concentrations toward local equilibrium with time. If the time increment Δt is too large, one overshoots local equilibrium disastrously. With an exponential decay, on the other hand, overshoot is impossible no matter how small the time constant.

In the following section we develop these ideas in more detail. This is followed by a section on results obtained with this model, showing how the line shapes depend on the various parameters in the model. These runs were made on a Zenith-150 microcomputer with a standard 8088 microprocessor running at 4.77 MHz. The program was written in BASICA and then compiled to give a fast-running machine language program; interpreted BASIC is too slow to be practical.

ANALYSIS

We shall use the model for gas chromatograph operation illustrated in Fig. 1. Initially we shall develop the local equilibrium theoretical plate treatment. Then we shall modify this by replacing the theoretical plate advection terms by one of three asymmetrical upwind algorithms yielding reduced numerical dispersion. Lastly, we shall modify the treatment to eliminate the assumption of local equilibrium, so that the kinetics of mass transport between phases can be included in the model.

We partition the column into N equal-sized compartments each of length Δx and radius r(cm). Let the voids fraction of the column be v_g, and the volume fraction of the liquid phase in the column be v_l. Let the volumetric flow rate of the carrier gas be v mL/min. Then we obtain

$$dm_i/dt = v(c_{g,i-1} - c_{g,i}) \tag{7}$$

for the equation describing advective motion in the column. Here, m_i is

the moles of solute in the ith compartment and $c_{g,i}$ is the concentration of solute in the ith compartment (mol/cm^3). Let us assume the following isotherm for the partitioning of the solute between the liquid and vapor phases at equilibrium:

$$c_{l,i} = \frac{ac_{g,i}}{1 + c_{g,i}/c_g^0} \tag{8}$$

Here c_g^0 may be positive (isotherm concave downward) or negative (isotherm concave upward). Mass balance gives

$$m_i = V_l c_{li} + V_g c_{gi} \tag{9}$$

where

$$V_l = \pi r^2 \Delta x \cdot v_l \tag{10}$$

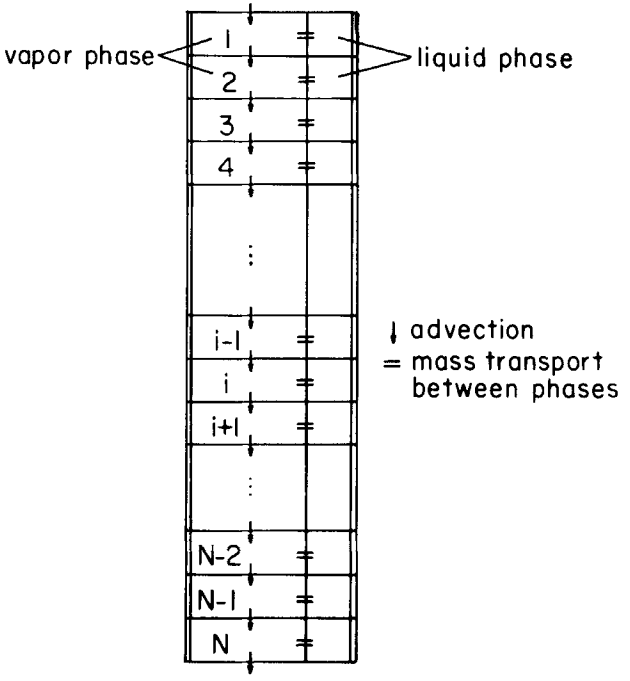

FIG. 1. The model used to represent the column.

$$V_g = \pi r^2 \Delta x \cdot v_g \tag{11}$$

Solving Eqs. (8) and (9) for $c_{g,i}$ in terms of m_i then yields

$$c_{g,i} = \frac{m_i - V_g c_g^0 - a V_l c_g^0 \pm \sqrt{(m_i - V_g c_g^0 - a V_l c_g^0)^2 + 4 V_g c_g^0 m_i}}{2 V_g},$$

$$i = 1, 2, \ldots, N \tag{12}$$

The positive sign is taken if c_g^0 is positive, the negative sign if c_g^0 is negative.

For the theoretical plate, local equilibrium model, Eqs. (7) are integrated forward in time numerically, with Eqs. (12) being used to calculate the changing values of the $c_{g,i}$. The value of $c_{g,0}$ is set equal to c_{inj} while sample injection is taking place; after this has occurred, it is set equal to zero.

This approach results in quite wide peaks due to the numerical dispersion intrinsic in the use of Eqs. (7) to model advection. We therefore replace the right-hand side of Eqs. (7) by one of the asymmetrical upwind algorithms, Eqs. (4), (5), or (6). For illustration, we choose Eq. (5), obtaining

$$\frac{dm_i}{dt} = v\left(-\frac{1}{8} c_{g,i-2} + \frac{7}{8} c_{g,i-1} - \frac{3}{8} c_{g,i} - \frac{3}{8} c_{g,i+1}\right) \tag{13}$$

We use Eq. (7) for $i = 1$ and N, since Eq. (13) requires nonexistent c_g's for these values of i.

At this stage we have recovered Tamamushi's work (*1*). It was found, however, that use of Eq. (13) or its congeners (obtained from Eqs. 4 or 6) under some circumstances resulted in more numerical instability than was desired. The peak was preceeded and/or followed by one or more wiggles which were obviously computational artifacts. This instability was reduced by combining Eq. (13) with the numerically highly stable but very dispersive Eq. (7), so that the differential equations representing advection become

$$\frac{dm_i}{dt} = v\left[b\left(-\frac{1}{8} c_{g,i-2} + \frac{7}{8} c_{g,i-1} - \frac{3}{8} c_{g,i} - \frac{3}{8} c_{g,i+1}\right) + (1 - b)(c_{g,i-1} - c_{g,i})\right] \tag{14}$$

[This device has proven effective in improving stability in the modeling

of ion-exchange columns (*13*).] Many of the results reported in the next section were calculated using Eqs. (12) and (14). This gives us a model which includes 1) an isotherm which can show positive or negative departures from Henry's law, and 2) the effects of the finite duration of the sample injection process. If one wishes to increase axial diffusion/dispersion, one can do so either by decreasing b in Eq. (14) or by decreasing N, the number of compartments into which the column is partitioned. It would also be possible to include a term

$$\frac{AD}{\Delta x}[c_{g,i-1} - 2c_{g,i} + c_{g,i+1}] \tag{15}$$

in Eq. (14) to include dispersion explicitly, but there appears to be little to be gained by this over what can be done by varying b and/or N.

The next problem to be addressed is that of including the effects of the finite rate of mass transfer of solute between the liquid and vapor phases. We assume that the decay of the concentrations toward their local equilibrium values is exponential; that these, in the absence of advection, would follow an equation of the form

$$c_{g,i}(t) = c^e_{g,i}(m_i) + [c_{g,i}(0) - c^e_{g,i}(m_i)] \cdot e^{-t/\tau} \tag{16}$$

where τ is the time constant for the decay toward equilibrium by mass transport between the liquid and vapor phases. Note that $c^e_{g,i}(m_i)$ is calculated from Eq. (12).

We modify our treatment of advection as follows. (For brevity the development is carried out with the theoretical plate advection algorithm; at the end we patch in an asymmetrical upwind algorithm.)

$$dm_i/dt = v(c_{g,i-1} - c_{g,i}) \tag{7}$$

$$\frac{dc_{g,i}}{dt} = \frac{v}{V_g}(c_{g,i-1} - c_{g,i}) \tag{17}$$

We use Eqs. (7) and (17) to calculate the increments in the m_i and the c_{gi} during the time interval Δt. Note that Eq. (17) includes no terms involving solute transport between phases. Therefore, the value of $c_{g,i}(\Delta t)$ calculated from Eq. (17) is *not* at equilibrium with the liquid phase; denote this value by $c^0_{g,i}(\Delta t)$. Next, use Eq. (16) to allow $c^0_{g,i}(\Delta t)$ to decay toward equilibrium; this yields

$$c_{g,i}(\Delta t) = c^0_{g,i}(\Delta t) + [c^e_{g,i}(m_i) - c^0_{g,i}(\Delta t)] \cdot [1 - \exp(-\Delta t/\tau)] \tag{18}$$

One integrates two sets of differential equations, Eq. (7) and Eq. (17), with the derivatives differing only by a constant factor, $1/V_g$. Then, each time increment, the values of the $c_{g,i}$ are allowed to relax toward the values they would have if local equilibrium were achieved with m_i moles of solute in the ith compartment, $i = 1, 2, \ldots, N$. Since the derivatives in Eqs. (7) and (17) are essentially identical and the exponential in Eq. (18) can be calculated before entering the main loop in the numerical integration, inclusion of mass transfer kinetics effects adds negligibly to the running time of the computer program integrating the differential equations.

To decrease numerical dispersion, one then replaces the theoretical plate advection algorithm in Eqs. (7) and (17) by the linear combination of algorithms used in Eq. (14). Also, the numerical integration was done by a two-step predictor-corrector method, with the relaxation toward equilibrium carried out with a factor $1 - \exp(-2\Delta t/\tau)$ in the predictor result and $1 - \exp(-\Delta t/\tau)$ in the corrector result. The predictor-corrector method used was of the form

Starter:

$$y^*(\Delta t) = y(0) + \frac{dy}{dt}(0)\Delta t \tag{19}$$

Predictor:

$$y^*(t + \Delta t) = y(t - \Delta t) + \frac{dy}{dt}(t) \cdot 2\Delta t \tag{20}$$

Corrector:

$$y(t + \Delta t) = y(t) + \left[\frac{dy^*}{dt}(t + \Delta t) + \frac{dy}{dt}(t)\right]\frac{\Delta t}{2} \tag{21}$$

The method is described in Ralston and Wilf (*16*).

The mass transport time constant can be estimated as follows. Assume that solute diffusion in the liquid phase is rate controlling, that the thickness of the liquid phase is l, and that l is sufficiently smaller than the packing dimensions that planar geometry can be used. Then we have the diffusion problem

$$\frac{\partial c}{\partial t} = D\frac{\partial^2 c}{\partial x^2} \tag{22}$$

$$\frac{\partial c}{\partial t}(0,t) = 0 \tag{23}$$

$$c(l,t) = c_0 \tag{24}$$

This problem is readily solved by separation of variables, and yields

$$c(x,t) = c_0 + \sum_{n=1}^{\infty} A_n \cos\left(\sqrt{\frac{\lambda_n}{D}}\, x\right) \cdot \exp(-\lambda_n t) \tag{25}$$

where

$$\lambda_n = [(2n - 1)\pi/2l]^2 D \tag{26}$$

We set the time constant τ equal to the reciprocal of the lowest nonzero eigenvalue, λ_1, which gives

$$\tau = (2l/\pi)^2/D \tag{27}$$

as an estimate of the time constant. Note that this neglects any diffusion effects in the gaseous boundary layer around a packing particle.

One can include the contribution from diffusion through the gaseous boundary layer in the following way. See Fig. 2 for the geometry and notation. The boundary conditions are as follows:

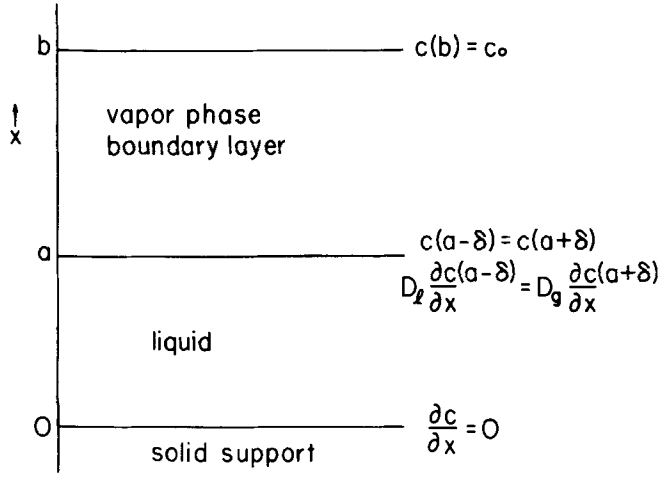

FIG. 2. Model for the kinetics of mass transport between phases.

$$\frac{\partial c}{\partial t}(0) = 0 \tag{28}$$

$$c(a - \delta) = Kc(a + \delta), \qquad \delta \to 0 \tag{29}$$

[At equilibrium, $c(x < a) = Kc(x > a]$

$$D_l \frac{\partial c}{\partial t}(a - \delta) = D_g \frac{\partial c}{\partial t}(a + \delta), \qquad \delta \to 0 \tag{30}$$

$$c(b) = c_0 \tag{31}$$

The diffusion equations in the two regions are

$$\frac{\partial c}{\partial t} = D_l \frac{\partial^2 c}{\partial t^2}, \qquad 0 < x < a \text{ (Region I)} \tag{32}$$

$$\frac{\partial c}{\partial t} = D_g \frac{\partial^2 c}{\partial t^2}, \qquad a < x < b \text{ (Region II)} \tag{33}$$

On taking Eq. (28) into account, it is easily shown that in Region I

$$c(x,t) = \sum_{\lambda} B_\lambda \exp(-\lambda t) \cos \sqrt{\frac{\lambda}{D_l}} x + Kc_0 \tag{34}$$

and in Region II we find

$$c(x,t) = \sum_{\lambda} \left[C_\lambda \cos \sqrt{\frac{\lambda}{D_g}} x + D_\lambda \sin \sqrt{\frac{\lambda}{D_g}} x \right] \exp(-\lambda t) + c_0 \tag{35}$$

Fitting the boundary conditions at $x = a$ gives

$$K^{-1} B_\lambda \cos \sqrt{\frac{\lambda}{D_l}} a = C_\lambda \cos \sqrt{\frac{\lambda}{D_g}} a + D_\lambda \sin \sqrt{\frac{\lambda}{D_g}} a \tag{36}$$

from Eq. (29), and

$$-\sqrt{\frac{\lambda}{D_l}} \sin \sqrt{\frac{\lambda}{D_l}} a B_\lambda = -\sqrt{\frac{\lambda}{D_g}} \sin \sqrt{\frac{\lambda}{D_g}} a C_\lambda + \sqrt{\frac{\lambda}{D_g}} \cos \sqrt{\frac{\lambda}{D_g}} a D_\lambda \tag{37}$$

from Eq. (30). Equation (31) yields

$$\cos\sqrt{\frac{\lambda}{D_g}}\,bC_\lambda + \sin\sqrt{\frac{\lambda}{D_g}}\,bD_\lambda = 0 \tag{38}$$

Nonzero solutions for these linear, homogeneous equations in B_λ, C_λ, D_λ, require that the determinant of their coefficients vanishes. This yields, after some reduction, the following equation for the eigenvalues

$$K^{-1}\sqrt{\frac{\lambda}{D_l}}\cos\sqrt{\frac{\lambda}{D_l}}\,a\cos\sqrt{\frac{\lambda}{D_g}}\,(b-a) - \sqrt{\frac{\lambda}{D_g}}\sin\sqrt{\frac{\lambda}{D_l}}\,a\sin\sqrt{\frac{\lambda}{D_g}}\,(b-a) = 0 \tag{39}$$

This equation must be solved numerically for λ; we take as our time constant τ the reciprocal of the smallest nonzero value of λ.

RESULTS

A program to compute this model was written in GW BASIC (essentially IBM's BASICA) and compiled. A representative run takes about 20 min on a Zenith 150 microcomputer. In most runs N, the number of compartments into which the column was partitioned, was set equal to 100. The parameter values for a standard run are given in Table 1; the parameters differing from these values are listed in the captions of the figures.

In Figs. 3 and 4 are shown two sets of runs, identical in all respects except that one is made using the theoretical plate algorithm (Eq. 7, Fig. 3); the other, using our modified upwind algorithm (Eq. 17, Fig. 4) with $b = 1.0$. It is immediately evident from the differences in the peak half-widths that the upwind algorithms permit one to reduce numerical dispersion very markedly below that resulting from the theoretical plate model. In Fig. 4 we also see some evidence of instability of the advection algorithm in the "wiggles" in the curves. These results are in agreement with Tamamushi's findings (*1*).

The effects of varying the sample size are shown in Figs. 5 and 6. In Fig. 5 the isotherm is of the Langmuir type, concave down, with $c_g^0 > 0$. We see the expected distortion of the peak symmetry (tailing to the right) with increasing sample size, as well as a shift to shorter retention times. Figure 6 shows peak shapes for various sample sizes when c_g^0 is negative, which causes positive deviations from Henry's law—an isotherm which is concave upward. Increasing sample size results in increasing asymmetry

TABLE 1
Parameters for the Standard Run

Column length, cm	200
Column diameter, cm	2
Column voids fraction	0.5
Column liquid fraction	0.05
Langmuir isotherm parameter a	25
Langmuir isotherm parameter c_g^0, mol/cm^3	10^{-3}
Mass transfer time constant τ, s	10^{-3}
Flow rate, cm^3/min	100
Injection concentration, mol/cm^3	10^{-3}
Duration of injection, min	0.1
Length of run, min	18
Δt, min	0.025
N	100
Upwind advection algorithm	Eq. (5)
Fractional contribution of upwind advection algorithm, b	0.9
Fractional contribution of theoretical plate advection algorithm, $1 - b$	0.1

of the peak, with tailing to the left; the retention time is also increased as sample size increases.

The effect of increasing the parameter a in the adsorption isotherm is illustrated in Fig. 7. Increasing a increases proportionately the solubility of the solute in the stationary phase, so should produce a proportional increase in retention time, as was found to be the case. The value of a should be proportional to the liquid phase loading of the column; the mass transfer time constant τ should be proportional to the square of the liquid phase loading, as seen from Eq. (27).

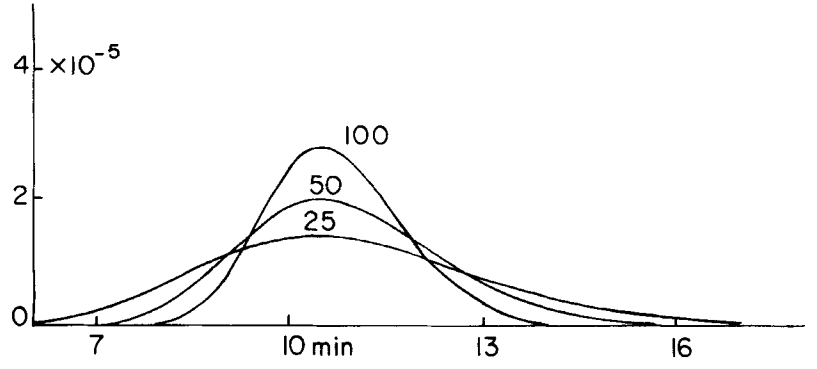

FIG. 3. Peak shapes obtained with the theoretical plate advection algorithm, Eq. (7). N = 25, 50, 100; other parameters as in Table 1.

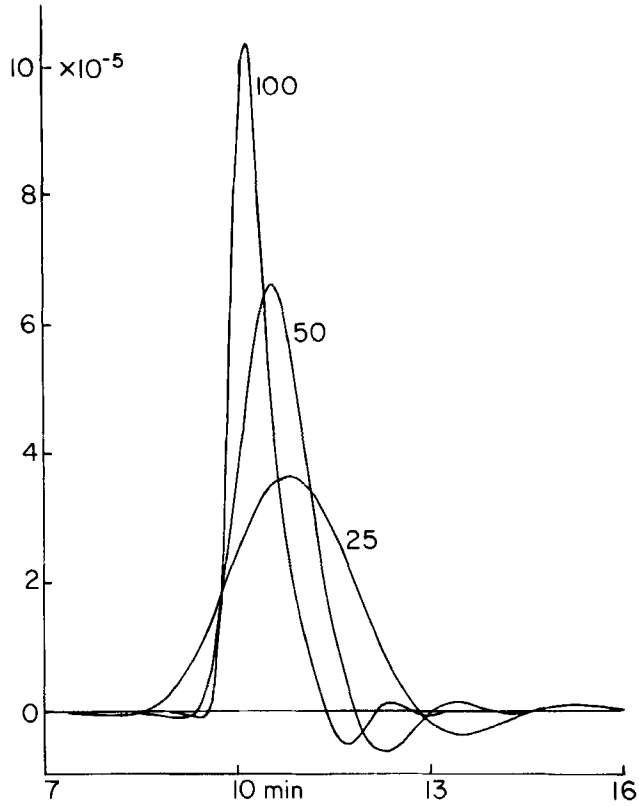

FIG. 4. Peak shapes obtained with a 4-point asymmetrical upwind algorithm for advection, Eq. (17). $N = 25, 50, 100$; $b = 0$; other parameters as in Table 1.

Increasing the duration of the injection time while holding total sample size constant causes the peaks to be broadened, as exhibited in Fig. 8. Slow vaporization of a large sample in the injection block would produce the same effect on peak shape.

The mass transfer time constant can be responsible for a good deal of peak broadening if the thickness of the stationary phase layer is sufficiently large, since τ is proportional to the square of this thickness. The extent of the broadening for various values of τ is shown in Fig. 9.

In Fig. 10 we explore the mathematical stabilities of our three asymmetrical upwind algorithms for the case where we have eliminated any contribution of the theoretical plate algorithm. [In the previous runs (except those in Figs. 3 and 4) we have included a 10% contribution from

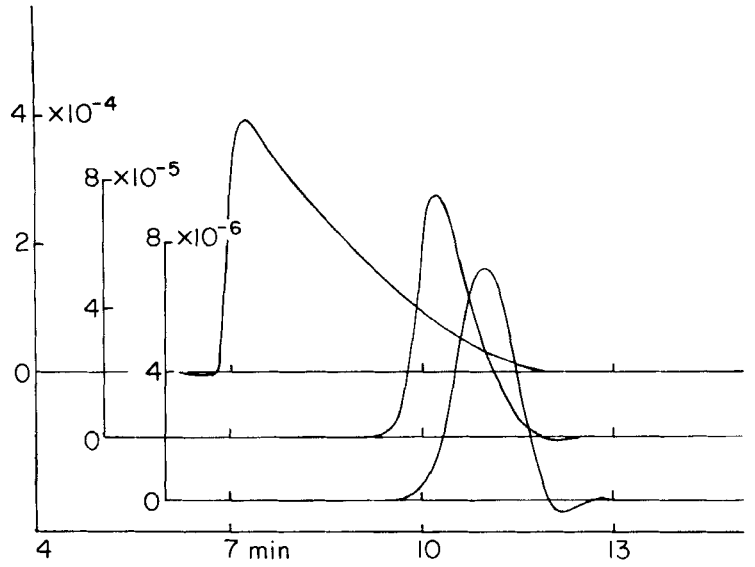

FIG. 5. Effect of sample size on peak shape with an isotherm showing negative departures from Henry's law. Injection concentrations = 10^{-4}, 10^{-3}, 10^{-2} mol/cm^3 right to left; other parameters as in Table 1.

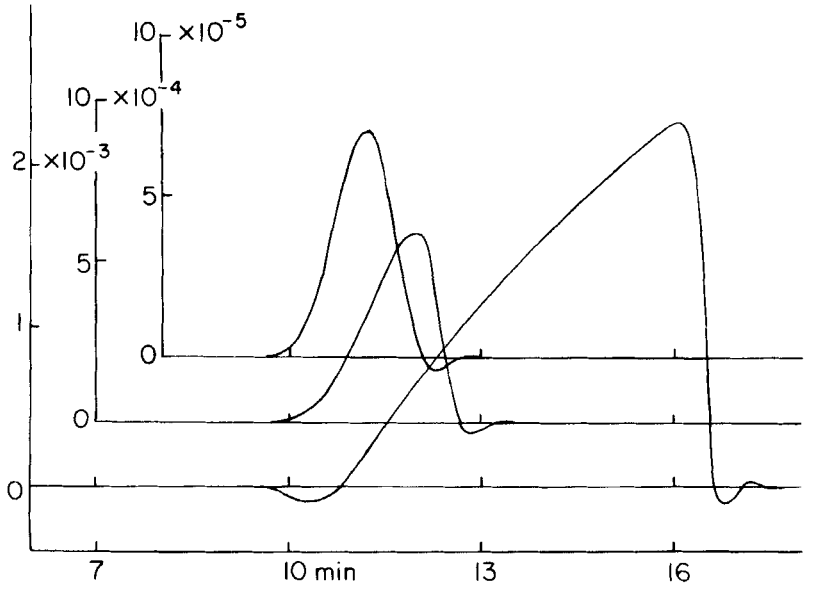

FIG. 6. Effect of sample size on peak shape with an isotherm showing positive departures from Henry's law. $c_g^0 = -0.01$ mol/cm^3; injection concentrations = 10^{-3}, 10^{-2}, 10^{-1} mol/cm^3 left to right; other parameters as in Table 1.

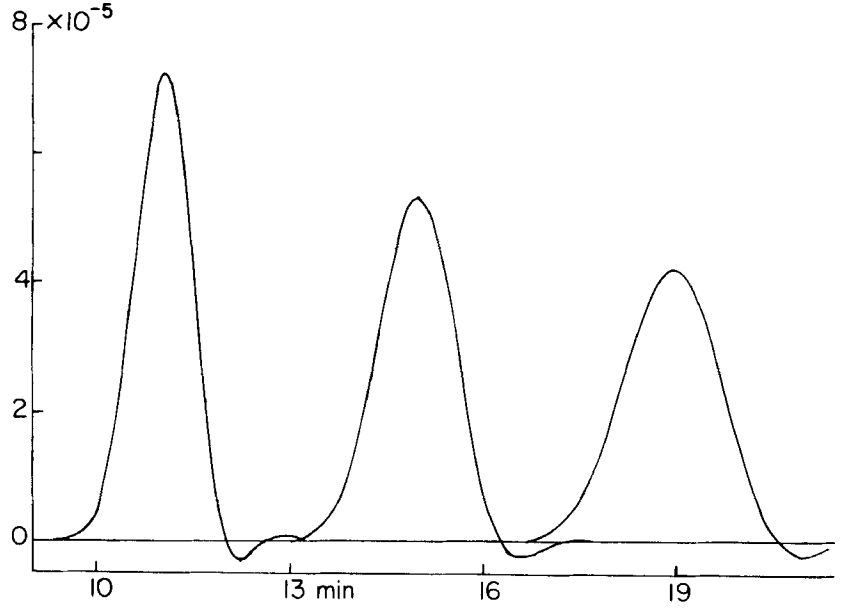

FIG. 7. Effect of the isotherm parameter a on peak shape. a = 25, 37.5, 50 (dimensionless) left to right; other parameters as in Table 1.

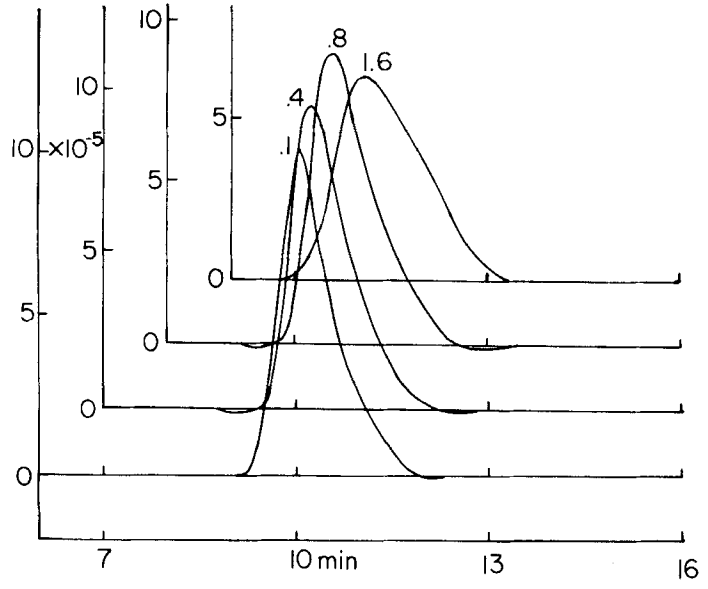

FIG. 8. Effect of injection time duration with constant sample size on peak shape. t_{inj} = 0.1, 0.4, 0.8, 1.6 min; $c_{inj} = 10^{-3}$, 2.5×10^{-4}, 1.25×10^{-4}, 6.25×10^{-5} mol/cm^3; other parameters as indicated in Table 1.

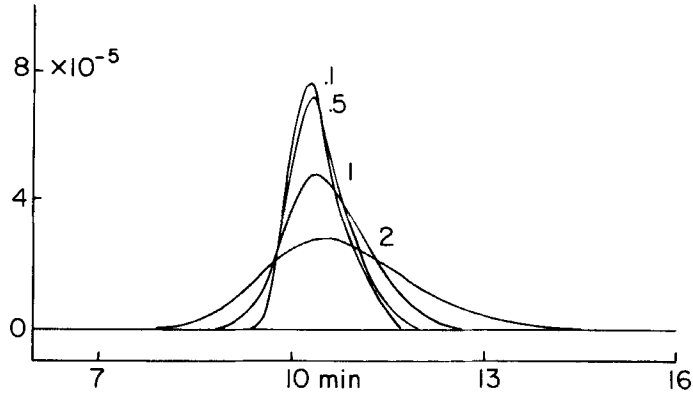

FIG. 9. Effect of mass transfer time constant τ on peak shape. τ = 0.1, 0.5, 1, 2 s (top to bottom); other parameters as in Table 1.

the theoretical plate algorithm to improve stability.] It is seen that the 3-point algorithm, Eq. (4), shows the most instability (indicated by the size of the spurious "wiggles" in the curve), and that the two 4-point algorithms are very similar to each other in this regard.

We note that most of the runs presented here, for which $N = 100$ and $t_{max} = 18$ min, took 20.4 min in compiled GW BASIC on our Zenith 150 microcomputer using a standard 8088 chip.

CONCLUSIONS

We conclude that it is possible to model the behavior of preparative gas chromatograph columns operating under conditions of sample overload and nonequilibrium mass transfer between the liquid and vapor phase, and that this can be carried out in reasonable time periods (of the order of 20 min per run) on a microcomputer using a compiled BASIC program.

Acknowledgments

This work was supported by a grant from the National Science Foundation. The author is indebted to Prof. Antonis D. Koussis for profitable discussions.

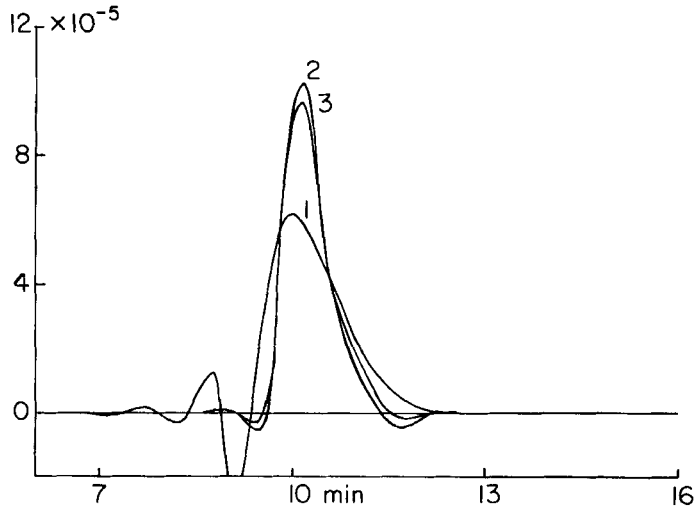

FIG. 10. Comparison of three asymmetrical upwind advection algorithms—their effects on peak shape. In all cases $b = 0$ (no contribution from the theoretical plate algorithm). The algorithms represented by Eqs. (4), (5), and (6) are used. Other parameters as in Table 1.

REFERENCES

1. K. Tamamushi and D. J. Wilson, *Sep. Sci. Technol., 21,* 339 (1986).
2. H. Vink, *J. Chromatogr., 20,* 496 (1965).
3. H. Vink, *Ibid., 24,* 39 (1966).
4. G. Houghton, *Ibid., 15,* 5 (1964).
5. J. C. Giddings, *J. Phys. Chem., 68,* 184 (1964) and earlier papers.
6. J. P. Muth, D. J. Wilson, and K. A. Overholser, *J. Chromatogr., 87,* 1 (1973).
7. S.-D. Huang, J. W. Wilson, D. J. Wilson, and K. A. Overholser, *Ibid., 89,* 119 (1974).
8. A. Jaulmes, C. Vidal-Madjar, A. Ladurelli, and G. Guiochron, *J. Phys. Chem., 88,* 5379 (1984).
9. B. P. Leonard, *Comput. Methods Appl. Mech. Eng., 19,* 59 (1979).
10. B. P. Leonard, in *Finite Element Methods for Convection Dominated Flows* (T. J. R. Hughes, ed.), American Society of Mechanical Engineers, New York, 1979.
11. K. C. Carter Jr., M. Saenz, D. J. Wilson, and P. W. Rosten Jr., *Environ. Monitor. Assess., 4,* 171 (1984).
12. W. Abraham and D. J. Wilson, *Ibid.,* In Press.
13. D. J. Wilson, *Sep. Sci. Technol.,* submitted.
14. D. J. Wilson, *Ibid., 17,* 1281 (1982).
15. D. J. Wilson and K. T. Valsaraj, *Ibid., 17,* 1387 (1983).
16. A. Ralston and H. S. Wilf, *Mathematical Methods for Digital Computers,* Vol. 1, Wiley, New York, 1965, p. 98.

Received by editor January 31, 1986